RSC Advances

ROYAL SOCIETY OF CHEMISTRY

www.rsc.org/advances

Journal Name

ARTICLE

Linking photoluminescence of α-Si_3N_4 to intrinsic point defects via band structure modelling

Received 29th August 2015,
Accepted XXth XX 20XX

DOI: 10.1039/x0xx00000x

www.rsc.org/

Zhifeng Huang,[a] Fei Chen,*[ab] Qiang Shen[a] and Lianmeng Zhang[a]

Photoluminescence (PL) property data for up-to-date reported α-Si_3N_4 are scattered and it is difficult to clarify the reason only through the experimental study. In this paper, the relationship between photoluminescence and intrinsic point defects in α-Si_3N_4 has been established accordingly via band structure modelling based on density functional theory calculation. The results show that band structures of α-Si_3N_4 are significantly affected by locations of defect levels, which are changed with various partial atomic structures around point defects. Formation energies are also calculated to determine main types of intrinsic point defects in α-Si_3N_4 under different conditions (Si-rich or N-rich). The results suggest that multiple types of intrinsic point defects coexist in α-Si_3N_4, leading to various electronic transition modes. Furthermore, combined with the calculated results, the discrete photoluminescence data for α-Si_3N_4 are revealed by electronic transition modes under different conditions. The main visible luminescent peaks for α-Si_3N_4 are attributed to the electron transitions of $E_c \rightarrow \equiv Si^{\bullet}\ \sigma$, and $\equiv Si^{\bullet}\ \sigma \rightarrow E_v$ for Si abundant α-Si_3N_4, while $N_4^{+} \rightarrow N_2^{0}$ for N plentiful α-Si_3N_4.

1. Introduction

Silicon nitride (Si_3N_4) is a wide band gap (~ 5.0 eV) semiconductor materials,[1,2] which has been drawn much attention in the optoelectrical fields for its significant visible luminescence properties due to the wide defect levels.[3-5] There are four types of defects in intrinsic point defect Si_3N_4: N dangling bond ($=N^{\bullet}$), Si dangling bond ($\equiv Si^{\bullet}$), Si–Si and N–N bonds.[6-11] The $=N^{\bullet}$ forms two defect levels in the band gap, namely N_2^{0} and N_4^{+}, which are near the top of valence band (VB) and the bottom of conduction band (CB), respectively.[7,8] The $\equiv Si^{\bullet}$ forms one defect level at about the middle of band gap according to the previous works.[6-9] However, recent work shows the defect levels of $\equiv Si^{\bullet}$ can be either occupied or unoccupied in the band gap by L. E. Hintzsche.[10] The Si–Si bond forms an occupied σ state close or on the top of VB and an empty σ^{*} state close or on the bottom of CB, and the N–N bond gives rise to a filled state in the VB and an empty state in the CB.[6-9] Nevertheless, the majority of published studies on related defects have been primarily focused on nonstoichiometric amorphous SiN_x films or clusters rather than bulk crystals.[6-11]

Density functional theory (DFT) offers an effective method to investigate physical properties for bulk crystals.[12,13] A lot of efforts based on DFT have been put on the mechanical, thermodynamic, optical and electronic properties for crystalline Si_3N_4.[14-20] Crystalline Si_3N_4 has two stable polymorphs at atmospheric environment, i.e. α-Si_3N_4 (trigonal, space group *P*31*c*) and β-Si_3N_4 (hexagonal, space group $P6_3$). α-Si_3N_4 is dynamically metastable phase under low temperature, and its periodic stacking structure of Si and N atoms is …ABCDABCD…, which is relatively complicated compared to …ABAB… for β-Si_3N_4.[17-18] Defect structures and electronic properties have been reported for intrinsic defects of β-Si_3N_4,[19-20] while little for α-Si_3N_4. Besides, the types of defects are mostly affected by the growth conditions.[21] Herein, to make clear the main point defect types in α-Si_3N_4 under different conditions, the formation energies for α-Si_3N_4 with different types of intrinsic point defects under N-rich and Si-rich conditions are calculated in this work.

To date, the photoluminescence properties for crystalline α-Si_3N_4 are experimentally diverse due to the electron transition mechanisms still unclear.[22-25] For instance, the luminescence peak for α-Si_3N_4 at ~ 600 nm (~ 2.1 eV) could be explained by electron transition of $N_4^{+} \rightarrow N_2^{0}$ by F. Gao,[25] or $E_c \rightarrow \equiv Si^{\bullet}$ by Y. Liu.[26] Some researchers concluded that the electron transition of $E_c \rightarrow \equiv Si^{\bullet}$ or $\equiv Si^{\bullet} \rightarrow E_v$ could form the emission peaks between 2.3 eV and 2.6 eV,[8,27] which is in conflict with the points that the $\equiv Si^{\bullet} \rightarrow E_v$ produce the peaks at about 3.0 eV.[28,29] Moreover, the $=N^{\bullet}$ would be grabbed by any surplus Si atom, in other words, the $=N^{\bullet}$ do not coexist with the $\equiv Si^{\bullet}$.[10] It is controversial to consider the $=N^{\bullet}$ and $\equiv Si^{\bullet}$ simultaneously in the same system to explore the electron transition mechanism.[28,29] Therefore, lacking investigations of band structures for intrinsic point defects of α-Si_3N_4 is the main reason resulting in diverse explanations for electron transition mechanisms.

[a] State Key Lab of Advanced Technology for Materials Synthesis and Processing, Wuhan University of Technology, Wuhan 430070, China.
[b] Massachusetts Institute of Technology, 77 Massachusetts Avenue, W20-021 Cambridge, MA 02139-4307, USA.
E-mail: chenfei027@gmail.com. Tel: +86-27-87168606; Fax: +86-27-87879468

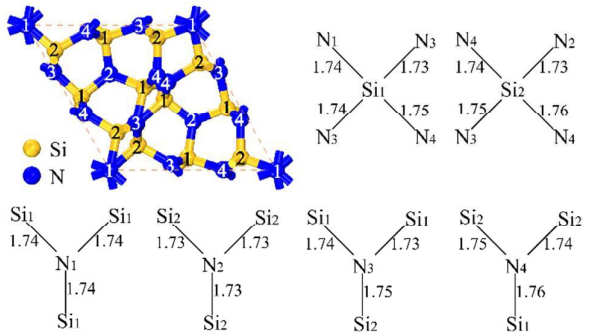

Fig. 1 Schematic diagram for different types of atoms in perfect α-Si_3N_4. The unit of bond length is Å.

In this paper, we devotes to link photoluminescence properties of α-Si_3N_4 to intrinsic point defects via band structure modelling based on DFT calculation. The intrinsic point defects: Si vacancy (V_{Si}), N vacancy (V_N), N substitutional to Si (Si_N), Si substitutional to N (N_{Si}), Si interstitial (Si_i) and N interstitial (N_i) are systematically considered. Firstly, the geometry optimizations for α-Si_3N_4 with intrinsic point defects are carried out to study the partial atomic environments near the point defects. Secondly, the electronic properties are calculated with the hybrid Heyd-Scuseria-Ernzerhof (HSE06) functional[30,31] to illustrate the influences of different intrinsic point defects on the band structures in α-Si_3N_4. Thirdly, the formation energies are calculated to determine the main types of intrinsic point defects in α-Si_3N_4 under the N-rich and Si-rich conditions, respectively. Finally, combined with the calculated results, the electron transitions contributing to the photoluminescence peaks are discussed for Si abundant and N plentiful α-Si_3N_4.

2. Theoretical and computational methods

The calculations were performed using CASTEP package based on the plane wave pseudo potential approach.[32] The optimized structures are obtained with the exchange-correlation functional was Perdew Burke Ernzerhof (PBE) of the generalized gradient approximation (GGA).[33] Then, the band structures and density of states were conducted by the HSE06 hybrid functional. To guarantee the calculation accuracy and efficiency, the 2 × 2 × 1 α-Si_3N_4 supercells with intrinsic point defects were calculated in this paper. A plane-wave cutoff energy of 400 eV and a *k*-point mesh of 3 × 3 × 5 were used. Reference configurations for the valence electrons were Si 3*s* 3*p* and N 2*s* 2*p*. The threshold for self-consistent field iterations was 1.0 × 10^{-5} eV per atom. The convergence tolerance parameters of optimized calculation were the energy of 2 × 10^{-5} eV per atom, the maximum force of 0.05 eV Å, the maximum inner stress of 0.1 GPa and the maximum displacement of 2 × 10^{-4} nm.

The lattice parameters and the density of states (DOS) of perfect α-Si_3N_4 supercells were calculated to validate the calculation schemes. The optimized lattice parameters are: a = b = 7.78 Å and c = 5.64 Å, and the calculated energy gap (E_g) by

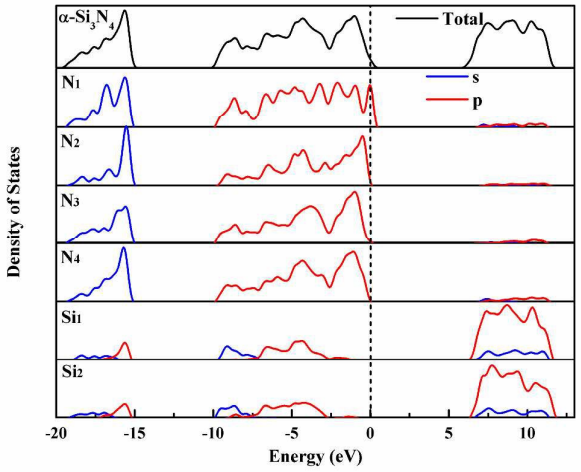

Fig. 2 Total and partial density of states for different atoms in perfect α-Si_3N_4.

HSE06 hybrid functional is 5.37 eV, which are in good agreement with the experimental value.[2] Through analyzing the types of atoms and bond lengths, there are two types of Si atoms (Si_1 and Si_2) and four types of N atoms (N_1, N_2, N_3 and N_4) in α-Si_3N_4, as shown in Fig. 1. It is seen from Fig. 1 that the Si–N bond lengths of N_1 and N_2 are the same, respectively. The total and partial DOS of different atoms in perfect α-Si_3N_4 are plotted in Fig. 2, where the Fermi levels (E_F) are set at 0 eV as the dashed lines. It is observed clearly from Fig. 2 that the contributions to the total DOS of the Si_1 and Si_2 are almost the same, as well as the N_3 and N_4. Note that the peak on the top of VB for the total DOS is main composed with N *pπ* states and its width depends on the second-neighbor N–N (*pσ*) interactions.[6] Different to the other types of N atoms, the tailing of the VB for the N_1 is significantly beyond the E_F resulting from the much larger *pσ* interactions for its planar configuration. The calculated DOS results are consistent with the previous calculations.[6,34] The above calculated results for perfect α-Si_3N_4 supercells confirm that our calculation schemes are reliable.

Considering there are two different Si atoms and four different N atoms in perfect α-Si_3N_4, six different vacant and six different substituted α-Si_3N_4 supercells are taken into account. Besides, there is a big interstice between the AB layer and CD layer in α-Si_3N_4,[17,18] so that two interstitial α-Si_3N_4 supercells are also considered. α-Si_3N_4 with vacant defects, one atom (Si or N) removed, are marked as V_{Si1}-Si_3N_4 and V_{Si2}-Si_3N_4 for Si vacancy, while V_{N1}-Si_3N_4, V_{N2}-Si_3N_4, V_{N3}-Si_3N_4 and V_{N4}-Si_3N_4 for N vacancy. α-Si_3N_4 with substitutional defects, one atom (Si or N) in the forms of a substitutional atom (Si_N or N_{Si}), are marked as Si_{N1}-Si_3N_4, Si_{N2}-Si_3N_4, Si_{N3}-Si_3N_4 and Si_{N4}-Si_3N_4 for Si substituting to N, while N_{Si1}-Si_3N_4 and N_{Si2}-Si_3N_4 for N substituting to Si. α-Si_3N_4 with interstitial defects, one atom (Si or N) occupying the interstice, are marked as Si_i-Si_3N_4 and N_i-Si_3N_4, respectively. After finishing geometry optimizations of all α-Si_3N_4 supercells with intrinsic point defects by the

Table 1 Optimal lattice parameters and lengths of new bonds for α-Si_3N_4 with intrinsic point defects.

Point defect	Cell parameter (Å)			Length of new bond (Å)		
	a	*b*	*c*	Si–N	Si–Si	N–N
V_{Si1}	7.83	7.83	5.63			
V_{Si2}	7.84	7.78	5.63			
V_{N1}	7.75	7.78	5.63		2.70	
					2.76	
V_{N2}	7.75	7.78	5.64		2.58	
					2.70	
V_{N3}	7.79	7.76	5.65		2.56	
V_{N4}	7.76	7.78	5.65		2.58	
Si_{N1}	7.86	7.86	5.62		2.16(3) [a]	
Si_{N2}	7.82	7.82	5.43		2.21(3) [a]	
Si_{N3}	7.79	7.82	5.66		2.15	
					2.19	
					2.21	
Si_{N4}	7.85	7.84	5.67		2.10	
					2.11	
					2.12	
N_{Si1}	7.78	7.74	5.65			1.41
						1.45(2) [a]
N_{Si2}	7.77	7.79	5.65			1.42
						1.45(2) [a]
Si_i	7.79	7.80	5.64	2.10	2.32	
				2.21	2.56	
				2.36		
N_i	7.79	7.81	5.65	1.81		1.59

[a] The numbers in the parentheses show the number of bonds with same length.

functional of GGA, the electronic properties are calculated with the HSE06 hybrid functional.

3. Results and discussion

3.1 Optimal crystal structures of α-Si_3N_4 with intrinsic point defects

Table 1 shows the lattice parameters and lengths of the new bonds for the optimal α-Si_3N_4 supercells with different intrinsic point defects. The variations of lattice parameters for α-Si_3N_4 with intrinsic point defects come from the changes of the partial atomic environments near the point defects. The partial atomic structures near the investigated point defects in α-Si_3N_4 are presented in Fig. 3. For α-Si_3N_4 with Si vacant defect (shown in Fig. 3 (a) and (b)), the distances become larger between each two N atoms compared with that of ~ 2.80 Å in perfect α-Si_3N_4, and no new bond is formed around the Si vacancy, leaving four unsaturated N dangling bonds (=$N^{\bullet}$). For α-Si_3N_4 with N vacant defect, the three nearest Si atoms are not equivalent,[16] with slightly shortening the distances of them (the distance of two nearest Si atoms is 2.96 Å in perfect α-Si_3N_4), to form two Si–Si bonds in the V_{N1}-Si_3N_4 and V_{N2}-Si_3N_4 (shown in Fig. 3 (c) and (d)), one Si–Si bond in the V_{N3}-Si_3N_4 and V_{N4}-Si_3N_4 (shown in Fig. 3 (e) and (f)), respectively. For α-Si_3N_4 with Si substituting to N defect (shown in Fig. 3 (g), (h), (i) and (j)), the substitutional Si atom forms three Si–Si bonds with its ambient Si atoms, and the extra electron of the substitutional Si atom forms one Si dangling bond (≡$Si^{\bullet}$).[19] It could be observed that the lengths of the three Si–Si bonds are the same in the Si_{N1}-Si_3N_4 and Si_{N2}-Si_3N_4 (shown in Fig. 3 (g) and (h)) while different in the Si_{N3}-Si_3N_4 and Si_{N4}-Si_3N_4 (shown in Fig. 3 (i) and (j)), attributed to different coordination environments of different types of N atoms, as shown in Fig. 1. For α-Si_3N_4 with N substituting to Si defect, the substitutional N atom forms three N–N bonds with its adjacent N atoms and leaves an unsaturated matrix N atom to form one N dangling bond (shown in Fig. 3 (k) and (l)). For α-Si_3N_4 with Si interstitial defect (shown in Fig. 3 (m)), the interstitial Si atom forms two strong Si–Si bond and three weak Si–N bonds with the matrix atoms.[20] For α-Si_3N_4 with interstitial N defect, the unsaturated interstitial N atom forms one N–N bond and one new Si–N bond with the matrix Si and N atoms (shown in Fig. 3 (n)). Compared with the optimized partial structures of all defective models, the V_{Si1}-Si_3N_4 and V_{Si2}-Si_3N_4, as well as the V_{N3}-Si_3N_4 and V_{N4}-Si_3N_4, the Si_{N3}-Si_3N_4 and Si_{N4}-Si_3N_4, as well as the N_{Si1}-Si_3N_4 and N_{Si2}-Si_3N_4 are almost the same. The main types of defects in α-Si_3N_4 with different intrinsic point defects are clearly illustrated by the partial atomic structures, whereas the electronic properties associated with the defects are discussed in the next section.

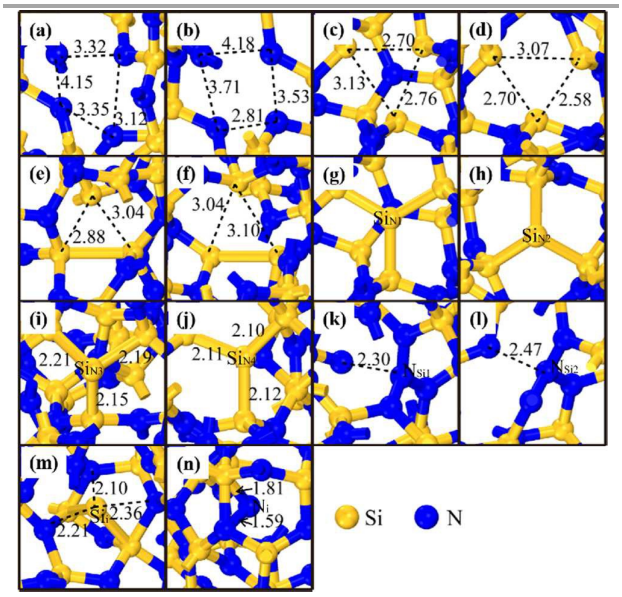

Fig. 3 Optimal partial atomic structures for α-Si_3N_4 with intrinsic point defects: (a) V_{Si1}, (b) V_{Si2}, (c) V_{N1}, (d) V_{N2}, (e) V_{N3}, (f) V_{N4}, (g) Si_{N1}, (h) Si_{N2}, (i) Si_{N3}, (j) Si_{N4}, (k) N_{Si1}, (l) N_{Si2}, (m) Si_i, (n) N_i. The unit of distance between the two atoms is Å.

3.2 Band structures of α-Si_3N_4 with intrinsic point defects

The calculated band structures and partial density of states (PDOS) of the atoms adjacent to the investigated point defects for all defective α-Si_3N_4 are plotted in Fig. 4, where the Fermi levels (E_F) are set at 0 eV as the red dashed lines. It is clear that the band structures and PDOS of the V_{Si1}-Si_3N_4 and V_{Si2}-Si_3N_4 (shown in Fig. 4 (a) and (b)), the V_{N3}-Si_3N_4 and V_{N4}-Si_3N_4 (shown

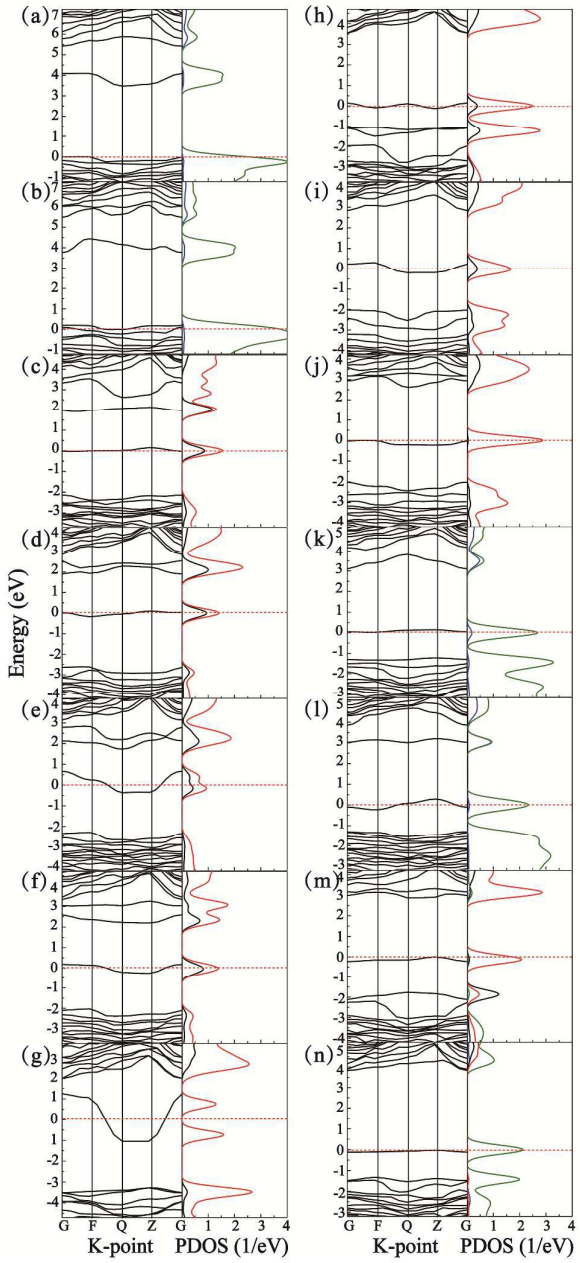

Fig. 4 Band structures and PDOS for α-Si_3N_4 with intrinsic point defects: (a) V_{Si1}, (b) V_{Si2}, (c) V_{N1}, (d) V_{N2}, (e) V_{N3}, (f) V_{N4}, (g) Si_{N1}, (h) Si_{N2}, (i) Si_{N3}, (j) Si_{N4}, (k) N_{Si1}, (l) N_{Si2}, (m) Si_i, (n) N_i. For the PDOS, the solid black lines stand for Si 3s, red for Si 3p, blue for N 2s and green for N 2p.

in Fig. 4 (e) and (f)), the Si_{N3}-Si_3N_4 and Si_{N4}-Si_3N_4 (shown in Fig. 4 (i) and (j)), as well as the N_{Si1}-Si_3N_4 and N_{Si2}-Si_3N_4 (shown in Fig. 4 (k) and (l)) are similar, respectively. Compared with the E_g = 5.37 eV for perfect α-Si_3N_4, the maximum energy gaps for all intrinsic defective α-Si_3N_4 become smaller owing to the emergence of defect levels in the band gaps. The E_v and E_c stand for the energies of the top of VB and the bottom of CB, respectively. The energies of N 2*s* and 2*p* states appear in the

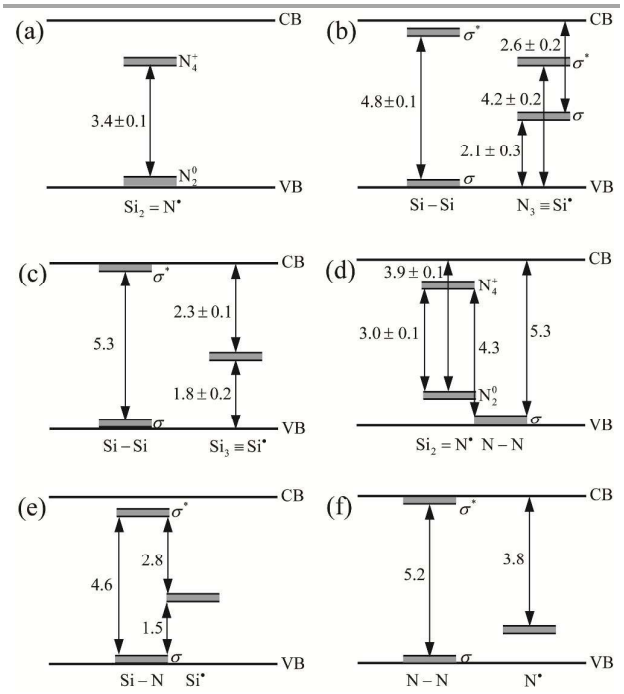

Fig. 5 Defect levels and electron transition diagrams in α-Si_3N_4 with intrinsic point defects: (a) V_{Si}, (b) V_N, (c) Si_N, (d) N_{Si}, (e) Si_i and (f) N_i. The unit of energy gap is eV.

E_v and just below the E_c in the V_{Si1}-Si_3N_4 and V_{Si2}-Si_3N_4, respectively, which are in good agreement with the results of Robertson's research,[6,7] indicating that N_2^0 and N_4^+ are the main defects in α-Si_3N_4 with Si vacant defect. For α-Si_3N_4 with N vacant defect, the defect levels located in the E_v and below the E_c are related to the Si–Si bonding σ states and antibonding σ^* states,[6-9] and the else two defect levels in the band gaps are the Si dangling bonds occupied ($N_3{\equiv}Si^\bullet$ σ) and unoccupied ($N_3{\equiv}Si^\bullet$ σ^*) states.[10] Particularly, for the V_{N1}-Si_3N_4 (see Fig. 4 (c)), owing to the lower energy of the Si–Si σ compared with the $p\sigma$ state, the defect level of the Si–Si σ state is certainly lower than the E_v. Besides, for the V_{N2}-Si_3N_4 (see Fig. 4 (d)), because the short distances between the three Si atoms adjacent to the N vacancy, the unsaturated Si dangling bond are not entirely separated from the Si–Si bonds, causing the overlapping of the $N_3{\equiv}Si^\bullet$ σ^* and Si–Si σ^* states. The distortion of the local Si environment and the Si–Si bond length could influence the location and composition of the electronic states of Si defect in the band gap.[10] Unlike the long lengths of Si–Si bonds in α-Si_3N_4 with N vacancy defect, the Si–Si bonds are particularly short and the three Si–Si bonds are closely around the unsaturated Si dangling band ($Si_3{\equiv}Si^\bullet$) in α-Si_3N_4 with Si substituting to N defect, resulting in the difference in the locations and compositions of Si–Si bonds and $Si_3{\equiv}Si^\bullet$. Thus, for α-Si_3N_4 with Si substituting to N defect, the defect levels close or in the E_v and the E_c are corresponding to the Si–Si σ and σ^* states, respectively, and the levels near the E_F are the $Si_3{\equiv}Si^\bullet$. As reported in Robertson's research, the N–N bond is mainly consisted of N 2*p* states and appearing in the VB or CB.[6] So the defect levels in the E_v are the N–N states, and the two defect

levels in the band gap are the N_2^0 and N_4^+ for α-Si_3N_4 with N substituting to Si defect. Similarly, for the N_i-Si_3N_4 (shown in Fig. 4 (n)), the defect levels composed of N 2*p* states in the VB and CB are the N–N σ and σ^* states, and the defect level near the E_F is the unsaturated N dangling bond state. For the Si_i-Si_3N_4 (shown in Fig. 5 (m)), the defect levels are consisted with N 2*p* and Si 3*s* 3*p* states in the VB and close to the E_c, which are related to the new Si–N bonds,[20] and the defect level near the E_F is the unsaturated Si dangling bond.

Considering the similar electronic properties for α-Si_3N_4 with similar intrinsic point defects, Fig. 5 summarizes the defect levels in the band gaps and electron transition diagrams for α-Si_3N_4 with six main point defects, which are the Si vacant defect (V_{Si}), N vacant defect (V_N), Si substituting to N defect (Si_N), N substituting to Si defect (N_{Si}), interstitial Si defect (Si_i) and interstitial N defect (N_i). The similar types of defect levels in the band gaps are different for the six main point defective models. For example, it is observed from Fig. 5 (a) and (d) that the maximum energy gaps of the two N dangling bonds states are ~ 3.4 eV in the V_{Si}-Si_3N_4, while ~ 3.0 eV in the N_{Si}-Si_3N_4. The relative locations of the defect levels of the two Si–Si states integrally move up in the band gaps from the V_N-Si_3N_4 to Si_N-Si_3N_4, as shown in Fig. 5 (b) and (c). For the defect levels of the unsaturated Si dangling bonds, there are two levels in the band gap for the V_N-Si_3N_4 (shown in Fig. 5 (b)), while only one level located at about the E_F in the Si_N-Si_3N_4 and Si_i-Si_3N_4 (shown in Fig. 5 (c) and (e)), respectively. The variations for the relative locations of similar defect levels come from different partial atomic environments.[10] For instance, the nearby atoms of the unsaturated Si atoms are N atoms in the V_N-Si_3N_4, Si atoms in the Si_N-Si_3N_4, N and Si atoms in the Si_i-Si_3N_4, so that the locations of defect levels originated from the unsaturated Si dangling bands are different for α-Si_3N_4 with different intrinsic point defects. To further investigate the main defect types under different conditions, the formation energies of α-Si_3N_4 with different intrinsic point defects are discussed in the next section.

3.3 Formation energy of α-Si_3N_4 with intrinsic point defects

The stability of different intrinsic point defect α-Si_3N_4 can be determined by the value of formation energy ($E_f(q)$), which is obtained by the following formula:[20,21,35]

$$E_f(q) = E_{tot}(q) - n_{Si}\mu_{Si} - n_N\mu_N - qE_F$$

where $E_f(q)$ stands for the total energy of the intrinsic defective α-Si_3N_4 supercell, n_{Si} and n_N for the numbers of Si and N atoms in the supercell, μ_{Si} and μ_N for the chemical potentials of Si and N atoms, q for the change state and E_F for the Fermi energy, respectively. Note that the $E_f(q)$ is not fixed but depends on the growth condition, which can be changed from N-rich ($\mu_N = \mu(N_2)/2$ and $\mu_{Si} = (\mu(\alpha\text{-}Si_3N_4) - 4\mu_N)/3$) to Si-rich ($\mu_N = \mu_{bulk\text{-}Si}$ and $\mu_N = (\mu(\alpha\text{-}Si_3N_4) - 3\mu_{Si})/4$) conditions.[21] Table 2 exhibits the formation energies for all α-Si_3N_4 supercells with intrinsic point defects under different growth conditions in the neutral charge state (q = 0). It can be clearly seen from Table 2 that $E_f(q)$ is sensitive to the growing conditions. A low formation energy indicates a high equilibrium concentration of the corresponding intrinsic point defect, whereas a high energy implies that it does not occur spontaneously. Compared with the formation energies, under the Si-rich condition, the V_N-Si_3N_4, Si_N-Si_3N_4 and Si_i-Si_3N_4 are easily obtained, while under the N-rich condition, the N_{Si}-Si_3N_4, V_N-Si_3N_4, N_i-Si_3N_4 and V_{Si}-Si_3N_4 are easily formed, indicating multiple intrinsic point defects coexist in α-Si_3N_4 under different growth conditions. Moreover, the low formation energies of V_N-Si_3N_4 indicate that N vacant defect is easily formed whatever it is under the N-rich or Si-rich conditions, which confirms the view that the Si dangling bonds is the dominant defects in α-Si_3N_4.[20,36] Owing to the unsaturated N atom grabbed by any existing Si defect (Si–Si and ≡$Si^•$),[10] the N substituting to Si defect and the interstitial N defect do not coexist with the N vacant defect. To make it easy to understand, we define the cases that the atomic ratio of Si and N in α-Si_3N_4 is more than 3:4 as Si_3N_{4-x}, which includes V_N-Si_3N_4, Si_N-Si_3N_4 and Si_i-Si_3N_4. The other cases of Si:N < 3:4 are defined as $Si_{3-x}N_4$, which are N_{Si}-Si_3N_4, N_i-Si_3N_4 and V_{Si}-Si_3N_4. It is clear that Si_3N_{4-x} can be easily formed under Si-rich condition, while $Si_{3-x}N_4$ can be prepared under N-rich condition.

Table 2 Formation energies (eV) for α-Si_3N_4 with intrinsic point defects under different conditions.

Point defect	Si-rich	N-rich	Point defect	Si-rich	N-rich
V_{Si1}	11.02	7.69	Si_{N2}	4.61	10.47
V_{Si2}	11.04	7.71	Si_{N3}	5.25	11.12
V_{N1}	3.36	5.89	Si_{N4}	5.58	11.45
V_{N2}	3.37	5.90	N_{Si1}	11.60	5.76
V_{N3}	3.00	5.52	N_{Si2}	11.22	5.39
V_{N4}	3.32	5.85	Si_i	6.15	9.50
Si_{N1}	4.88	10.75	N_i	8.23	5.74

3.4 Linking photoluminescence of α-Si_3N_4 to intrinsic point defects

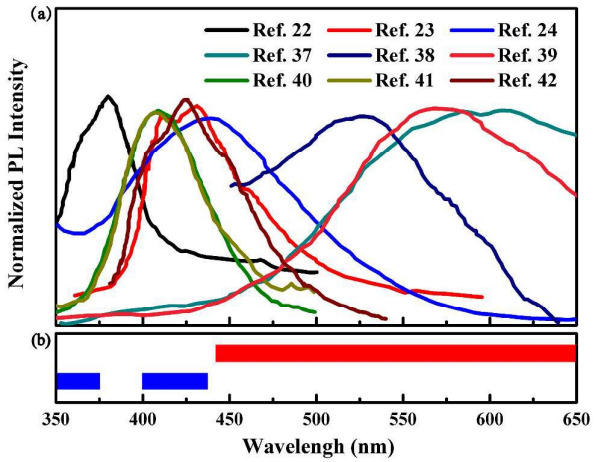

Fig. 6 (a) Photoluminescence data for α-Si_3N_4 in different literatures. (b) Wavelength ranges of the emission peaks for Si_3N_{4-x} (red bar) and $Si_{3-x}N_4$ (blue bars), respectively.

The currently reported photoluminescence data for α-Si_3N_4 are plotted Fig. 6 (a).[22-24,37-42] It is observed that the PL data is quite scattered, and PL properties are analyzed using different electron transition modes. The reason now is clear because there are multiple intrinsic point defects for Si_3N_{4-x} and $Si_{3-x}N_4$, determined by different experiment processing methods, resulting in different electron transition in the band gap, and correspondingly a number of visible luminescence peaks. Some of the broaden peaks may be the integral of several single peak, which reflects certain electron transition mode. According to previous analysis, it is known that for Si_3N_{4-x}, the E_v and E_c may be composed of the occupied and empty states of Si–Si or Si–N bond, as exhibited in Fig. 5 (b), (c) and (e), respectively. The defects levels in the band gap are related to the unsaturated Si dangling bonds (≡$Si^{\bullet}$), which may be in different forms as $N_3{\equiv}Si^{\bullet}$, $Si_3{\equiv}Si^{\bullet}$ or the other unsaturated Si states. On the other hand, for $Si_{3-x}N_4$, the E_v and E_c may be composed of the N–N occupied and empty states as exhibited in Fig. 5 (a), (d) and (f). The defect levels in the band gap are the unsaturated N dangling bonds (=$N^{\bullet}$).

The wavelength ranges of the emission peaks are shown as the red and blue bars in Fig. 6 (b) for Si_3N_{4-x} and $Si_{3-x}N_4$, respectively. Thus, it is clear that in the Si abundant α-Si_3N_4, the PL peaks at > 440 nm (the corresponding energy gaps < 2.8 eV) are related to the electron transitions of ≡$Si^{\bullet}$ $\sigma \rightarrow E_v$, or $E_c \rightarrow$ ≡$Si^{\bullet}$ σ. While in the N plentiful α-Si_3N_4, the PL peaks of 400 ~ 430 nm (2.8 ~ 3.0 eV) may be driven from the electron transitions of $N_4^+ \rightarrow N_2^0$, and the peaks at < 380 nm (> 3.3 eV) relate to $N_4^+ \rightarrow E_v$ in Si vacant α-Si_3N_4. For example, the main PL peaks located at > 500 nm[37-39] may be derived from the electron transitions of ≡$Si^{\bullet}$ $\sigma \rightarrow E_v$ or $E_c \rightarrow$ ≡$Si^{\bullet}$ σ, however, the main peaks at 410 ~ 430 nm[23,24,40-42] are related to the electron transitions of $N_4^+ \rightarrow N_2^0$. The current investigation has successfully demonstrate the reason for the discreteness of the PL spectra for α-Si_3N_4.

4. Conclusions

Photoluminescence properties of α-Si_3N_4 has been connected to intrinsic point defects by band structure modelling using DFT calculations. The partial atomic structures, electronic properties and formation energies for α-Si_3N_4 with different intrinsic point defects are systematically investigated. The Si dangling bonds give rise to two defect levels ($N_3{\equiv}Si^{\bullet}$ σ and σ^*) in the band gap for the V_N-Si_3N_4, while only one defect level for the Si_N-Si_3N_4 and Si_i-Si_3N_4. The maximum energy gaps between N_2^0 and N_4^+ are different in the V_{Si}-Si_3N_4 and N_{Si}-Si_3N_4. The different locations of the similar defect levels are originated from the various partial atomic environments adjacent to the investigated point defects. Multiple types of intrinsic point defects would coexist in α-Si_3N_4 under different environments derived from formation energy calculation. The main visible luminescent peaks for α-Si_3N_4 are attributed to the electron transitions of $E_c \rightarrow$ ≡$Si^{\bullet}$ σ, and ≡$Si^{\bullet}$ $\sigma \rightarrow E_v$ for Si_3N_{4-x}, while $N_4^+ \rightarrow N_2^0$ for $Si_{3-x}N_4$. This work not only reveals the discrete photoluminescence data for α-Si_3N_4, but also provides theoretical foundations for electronic properties of Si_3N_4.

Acknowledgements

The project is supported by the National Natural Science Foundation of China (No. 51202171, No. 51472188, No. 51521001), the Specialized Research Fund for the Doctoral Program of Higher Education of China (No. 20120143120004) and the “111” project (No. B13035).

Notes and references

1 K. Ulman, R. Sathiyanarayanan, R. K. Pandey, K. V. R. M. Murali and S. Narasimhan, *J. Appl. Phys.*, 2013, **113**, 234102.
2 L. Zhang, H. Jin, W. Yang, Z. Xie, H. Miao and L. An, *Appl. Phys. Lett.*, 2005, **86**, 1908.
3 R. J. Xie and N. Hirosaki, *Sci. Technol. Adv. Mat.*, 2007, **8**, 588-600.
4 J. Cai, Y. L. Zhang, Z. Y. Lyu, J. Zhao, J. C. Shen, Q. Wu and Z. Hu, *CrystEngComm*, 2015, **17**, 23-26.
5 B. Sain and D. Das, *Phys. Chem. Chem. Phys.*, 2013, **15**, 3881-3888.
6 J. Robertson, *Philos. Mag. B*, 1991, **63**, 47-77.
7 J. Robertson, *Mater. Res. Symp. Proc.*, 1993, **284**. 65-76.
8 S. V. Deshpande, E. Gulari, S. W. Brown and S. C. Rand, *J. Appl. Phys.*, 1995, **77**, 6534-6541.
9 J. Robertson, W. L. Warren and J. Kanicki, *J. Non-Cryst. Solids*, 1995, **187**, 297-300.
10 L. E. Hintzsche, C. M. Fang, M. Marsman, G. Jordan, M. W. P. E. Lamers, A. W. Weeber and G. Kresse, *Phys. Rev. B*, 2013, **88**, 155204.
11 P. A. Pundur, J. G. Shavalgin and V. A. Gritsenko, *Phys. Status Solidi A*, 1986, **94**, K107-K112.
12 S. Baroni, S. De Gironcoli, A. Dal Corso and P. Giannozzi, *Rev. Mod. Phys.*, 2001, **73**, 515.
13 J. Yu, P. Zhou and Q. Li, *Phys. Chem. Chem. Phys.*, 2013, **15**, 12040-12047.
14 D. Legut, U. D. Wdowik and P. Kurtyka, *Mater. Chem. Phys.*, 2014, **147**, 42-49.
15 G. Kresse, M. Marsman, L. E. Hintzsche and E. Flage-Larsen, *Phys. Rev. B*, 2012, **85**, 045205.

16 V. A. Gritsenko, S. S. Nekrashevich, V. V. Vasilev and A. V. Shaposhnikov, *Microelectron. Eng.*, 2009, **86**, 1866-1869.
17 A. Kuwabara, K. Matsunaga and I. Tanaka, *Phys. Rev. B*, 2008, **78**, 064104.
18 D. Hardie and K. H. Jack, *Nature*, 1957, **180**, 332.
19 C. Di Valentin, G. Palma and G. Pacchioni, *J. Phys. Chem. C*, 2010, **115**, 561-569.
20 M. E. Grillo, S. D. Elliott and C. Freysoldt, *Phys. Rev. B*, 2011, **83**, 085208.
21 F. Oba, K. Tatsumi, I. Tanaka and H. Adachi, *J. Am. Ceram. Soc.*, 2002, **85**, 97-100.
22 Z. Wu, Z. Zhang, J. Yun, J. Yan and T. You, *Physica B*, 2013, **428**, 10-13.
23 L. W. Lin and Y. H. He, *CrystEngComm*, 2012, **14**, 3250-3256.
24 J. Huang, S. Zhang, Z. Huang, Y. Wen, M. Fang and Y. Liu, *CrystEngComm*, 2012, **14**, 7301-7305.
25 F. Gao, W. Yang, Y. Fan and L. An, *Nanotechnology*, 2008, **19**, 105602.
26 Y. Liu, Y. Zhou, W. Shi, L. Zhao, B. Sun and T. Ye, *Mater. Lett.*, 2004, **58**, 2397-2400.
27 G. Zou, B. Hu, K. Xiong, H. Li, C. Dong, J. Liang and Y. Qian, *Appl. Phys. Lett.*, 2005, **86**, 1901.
28 H. Du and A. Gao, *Mater. Lett.*, 2012, **84**, 31-33.
29 Y. Xu, C. Cao, Z. Chen, J. Li, F. Wang and H. Cai, *J. Phys. Chem. B*, 2006, **110**, 3088-3092.
30 A. V. Krukau, O. A. Vydrov, A. F. Izmaylov and G. E. Scuseria, *J. Chem. Phys*, 2006, **125**, 224106.
31 J. Paier, M. Marsman, K. Hummer, G. Kresse, I. C. Gerber and J. G. Ángyán, *J. Chem. Phys.,* 2006, **124**, 154709.
32 M. C. Payne, M. P. Teter, D. C. Allan, T. A. Arias and J. D. Joannopoulos, *Rev. Mod. Phys.*, 1992, **64**, 1045.
33 J. P. Perdew, K. Burke and M. Ernzerhof, *Phys. Rev. Lett.*, 1996, **77**, 3865.
34 Y. N. Xu and W. Y. Ching, *Phys. Rev. B*, 1995, **51**, 17379.
35 Y. X. Han, C. L. Yang, M. S. Wang and X. G. Ma, *RSC Adv.*, 2014, **4**, 55452-55458.
36 J. Robertson and M. J. Powell, *Appl. Phys. Lett.*, 1984, **44**, 415-417.
37 M. Ahmad, J. Zhao, C. Pan and J. Zhu, *J. Cryst. Growth*, 2009, **311**, 4486-4490.
38 G. Zou, B. Hu, K. Xiong, H. Li, C. Dong, J. Liang and Y. Qian, *Appl. Phys. Lett.*, 2005, **86**, 1901.
39 L. W. Yin, Y. Bando, Y. C. Zhu and Y. B. Li, *Appl. Phys. Lett.*, 2003, **83**, 3584.
40 Y. Xu, C. Cao, H. Du, J. Li and H. Zhu, *Mater. Lett.*, 2007, **61**, 3855-3858.
41 Y. Xu, C. Cao, Z. Chen, J. Li, F. Wang and H. Cai, *J. Phys. Chem. B*, 2006, **110**, 3088-3092.
42 H. Du and A. Gao, *Mater. Lett.*, 2012, **84**, 31-33.